RSC Advances

ROYAL SOCIETY OF CHEMISTRY

www.rsc.org/advances

RSC Advances

COMMUNICATION

Enhanced photovoltaic characteristics of MoS_2/Si hybrid solar cells by metal Pd chemical doping

Received 00th January 2015,
Accepted 00th January 2015

DOI: 10.1039/x0xx00000x

www.rsc.org/advances

L. Z. Hao,[a,b*] Y. J. Liu,[b] W. Gao,[b] Y. M. Liu,[b] Z. D. Han,[b] Q. Z. Xue[b] and J. Zhu[c]

MoS_2/Si hybrid solar cells are fabricated and the device performances are improved via metal Pd chemical doping. Due to the incorporation of the Pd atoms in the MoS_2 films, the photovoltaic characteristics of the solar cell are enhanced significantly and a 375% enhancement of the power conversion efficiency can be obtained.

In recent years, molybdenum disulfide (MoS_2) has received much attention in the area of solar cells due to its high sunlight absorption.[1] Based on the configuration of Schottky or *p-n* junctions, several kinds of MoS_2-based solar cells were constructed.[2] For example, Wi et al. utilized the plasma-induced p-doping approach to form homojunctions in MoS_2 layers.[3] The devices showed good photovoltaic properties with a large short-circuit photocurrent density of 20.9 $mAcm^{-2}$ and power conversion efficiency (PCE) of 2.8%. To further improve the device performance and develop practically applicable photovoltaic devices, extensive efforts have been devoted to the fabrication of the heterojunctions by combining MoS_2 with other semiconductors, such as silicon (Si).[4] For example, Tsai et al. realized the increase of the PCE from 4.64% to 5.23% in Al/Si solar cells by stacking a MoS_2 monolayer on Si to enhance light absorption.[5] Further, a high PCE of 11.1% has been achieved in the graphene/MoS_2/Si solar cell.[6] It can be expected that the MoS_2/Si heterojunctions would become one of good candidates to develop high-performance solar cells. The previous studies are mainly focused on the solar cell devices composed of pure MoS_2 nanoscale materials without doping. However, there are few researches on photovoltaic characteristics of MoS_2 doped with metal elements. By the incorporation of suitable metal elements, the electrical and optical properties of MoS_2 could be increased.[7] Thus, the photovoltaic performance of the MoS_2 devices would be promoted.

In this work, MoS_2/Si solar cell devices are fabricated using magnetic sputtering technique and the device performances are improved via the metal palladium (Pd) chemical doping in the MoS_2 film. Pd is chosen as the dopant mainly based on the following three reasons. Firstly, stable substitution of the host Mo atoms with Pd atoms in MoS_2 could be formed due to their similar covalent radius (Mo=130 pm and Pd=128 pm).[8] Secondly, MoS_2 might be modulated from the *n*-type to the *p*-type because Pd has stronger electronegativity than Mo. Finally, the incorporation of Pd into the light sensitive layer can enhance the photovoltaic performance of the devices.[9] According to our measurements, the substitution of the host Mo atoms with the Pd dopants in the MoS_2 film is confirmed. Due to the chemical incorporation of the Pd atoms, the Pd:MoS_2/Si device show a significant enhancement of the photovoltaic performance with a 375% increase of the PCE.

1%Pd-doped MoS_2 (Pd:MoS_2) thin films were deposited on (100)-oriented Si substrates using dc magnetron sputtering technique. The Pd powders (purity, 99.9%) and MoS_2 powders (purity, 99.9%) with the molar ratio of 1:99 were firstly ball milled for 2 h and then the mixture was cold-pressed into disk as the sputtered target under 20 MPa. The (100)-oriented single Si substrates are *n*-type semiconductors with the resistivity of 3.2-6.8 Ω cm. The substrates were ultrasonically cleaned in sequence by alcohol, acetone, and de-ionized water. Then, the substrates were dipped into HF solution (~5%) for ~60 s to remove the natural oxide layer from the Si surface. After that, oxidation treatment were performed in H_2O_2 solution (~10%) at 100 °C to form a ~3.0-nm-thickness SiO_2 passivation layer on the Si surface. Subsequently, ~30-nm-thickness MoS_2 films were deposited. During the deposition, the working pressure and deposition temperature were 5.0 Pa and 400.0 °C, respectively. Finally, one ~40-nm-thickness Pd electrode layer was sputtered on the whole top surface of the film and indium (In) layer was covered on the whole backside of the Si. The thickness of the MoS2 film and the Pd top electrode layer were calibrated by Scanning Electron Microscope (SEM). As a reference, the device with the MoS_2 film was also fabricated.

Samples were characterized using Raman spectroscopy (Renishaw, 514 nm laser). X-ray photoemission spectroscopy (XPS) was performed by a Kratos Axis ULTRA spectrometer using a monochromatic Al Kα x-ray source (1486.6 eV). The transmission spectra were measured by Shimadzu UV-3150 spectrophotometer. Ultraviolet photoelectron spectroscopy (UPS) measurements were made using an unfiltered He-I (21.22 eV) gas discharge lamp. The current density-voltage (*J-V*) curves were measured using two-point

[a] College of Science, China University of Petroleum, Qingdao, Shandong 266580, China E-mail: haolanzhong@upc.edu.cn
[b] State Key Laboratory of Heavy Oil Processing, China University of Petroleum, Qingdao, Shandong 266580, China.
[c] State Key Laboratory of Electronic Thin Films and Integrated Devices, University of Electronic Science and Technology of China, Chengdu 610054, China

measurement by a Keithley2400 source meter under AM 1.5 illumination (100 mWcm^{-2}).

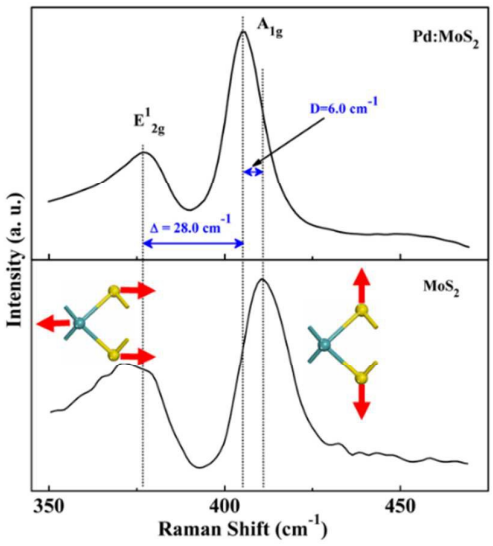

Fig. 1 Raman spectra of MoS_2 and Pd:MoS_2 films. The insets show the schematic illustrations of the oscillating modes of E^1_{2g} and A_{1g}, respectively. Atom color code: light blue-green, Mo; yellow, S.

Fig. 1 shows the Raman spectra of the MoS_2 and Pd:MoS_2 film. The MoS_2 film exhibits two characteristic Raman peaks, the E^1_{2g} mode at ~376 cm^{-1} and the A_{1g} mode at ~410 cm^{-1}. These results are consistent with other reported results.[10] The E^1_{2g} mode corresponds to the S and Mo atoms oscillating in antiphase parallel to the crystal plane and the A_{1g} mode corresponds to the S atoms oscillating in antiphase out-of-plane, as shown in the insets. From the figure, obvious red shift (D) of about 6.0 cm^{-1} of the A_{1g} peak can be observed after the Pd doping, while the position of the E^1_{2g} peak almost has no obvious change. The separation (Δ) between the E^1_{2g} and A_{1g} peaks decreases from 34.0 cm^{-1} of the pure MoS_2 film to 28.0 cm^{-1} of the doped film. In MoS_2-based materials, A_{1g} phonons couple much more tightly with electrons than E^1_{2g} phonons.[7] Hence, the change of the electronic structure and semiconductor characteristics of the film can be caused by the the Pd doping.

Fig. 2a shows the typical XPS spectrum of the Pd:MoS_2 film, illustrating the presence of Pd, Mo and S coexisted in the film. Fig. 2b provides the binding energies of Pd atoms in the Pd:MoS_2 film. Two peaks at 337.6 eV and 342.9 eV are assigned to Pd $3d_{5/2}$ and $3d_{3/2}$, respectively. The binding energies are much larger than those for Pd metals[11] and almost same with the characteristics of Pd^{4+}.[12] This reveals that the substitution of Mo atoms with Pd dopants is realized successfully and the Pd atoms are stabilized by covalent bonding inside the lattice. A typical high resolution XPS spectrum of Mo 3d and S 2p for the MoS_2 films with/without Pd doping are shown in Fig. 2c and d, respectively. The peaks at 229.1 eV and 232.1 eV are assigned to Mo $3d_{5/2}$ and Mo $3d_{3/2}$ orbital, respectively. As shown in the figure, the core-level peaks of Mo in the Pd:MoS_2 show a uniform shift toward lower binding energies compared to those for the undoped film. This shift can be attributed to the lowering of the Fermi level (E_F) upon the *p*-type doping, as similarly observed in previous studies.[13] According to the calculation, the amount of the shift of the binding energy is about 0.59 eV. The S $2p_{1/2}$ and S $2p_{3/2}$ appear at 163.5 and 162.2 eV, respectively, and there is almost no obvious difference between the binding energies for the films.

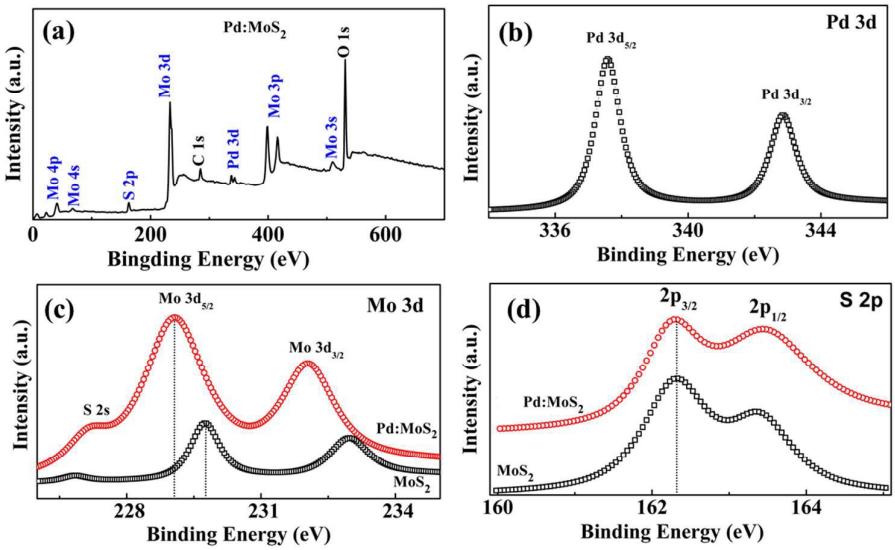

Fig. 2 (a) XPS spectrum of the Pd:MoS_2 film. (b) Binding energies of Pd 3d. (c) and (d) Comparison of Mo 3d and S 2p for the MoS_2 films with/without Pd doping.

Fig. 3a shows the schematic illustration of the measurement configuration for photovoltaic measurements. Here, forward voltages are defined as positive voltages applied on the Pd top electrode. The *J-V* curves of the devices with/without Pd doping were measured under the dark condition and AM 1.5 illumination, respectively. Fig. 3b shows the dark *J-V* curves of the devices. Obvious rectifying behaviors can be seen. The rectification ratio (J_+/J_-) at ±0.5 V reaches 10^2 order of magnitude for the devices. Besides the MoS_2/Si junction, Schottky contacts are likely to be formed at the Pd/MoS_2 interfaces according to other studies.[14] However, the ohmic contacts of Pd/MoS_2 are confirmed in our experiments.[15] Thus, the asymmetric characteristics originate

mainly from the MoS_2/Si and Pd:MoS_2/Si contacts, respectively. The turn-on voltage (V_{ON}) of 0.23 V for the undoped junction, at which the current starts to increase rapidly, can be obtained. From the figure, we can see that the V_{ON} increases to 0.47 V when the Pd dopants are incorporated into the film. The inset further shows the replots of the dark *J-V* curves in the reverse voltage range using semi-logarithmic mode. As shown in the figure, the decrease of the leakage current density (J_R) can be seen clearly after the doping. At -1.0 V, J_R=3.8×10^{-2} mAcm^{-2} for the doped device while 9.8×10^{-2} mAcm^{-2} for the undoped one. Fig. 3c shows the photovoltaic characteristics of the devices with/without the Pd doping. The undoped device shows an open-circuit voltage (V_{OC}) of 0.22 V and a short-circuit current density (J_{SC}) of 5.9 mAcm^{-2}, resulting in a PCE of 0.64%. After the Pd doping, the photovoltaic performance is enhanced significantly, as shown in the figure. For the Pd:MoS_2/Si solar cell, V_{OC} increases to 0.45 V, an enhancement of over 2 times. Simultaneously, J_{SC} increases to 15.1 mAcm^{-2}. The overall PCE reaches 2.4%, up to a 375% increase compared to the undoped device. Fig. 3d shows the corresponding incident photon-to-electron conversion efficiency (IPCE) curves of the devices. As shown in the figure, the IPCE values of the doped device are much larger than the undoped device in 300-1100 nm. This further demonstrates that the former has higher efficiencies on carrier collection. Thus, the incorporation of the Pd dopants into the film plays a crucial role to improve the light-to-current conversion efficiency for the fabricated devices.

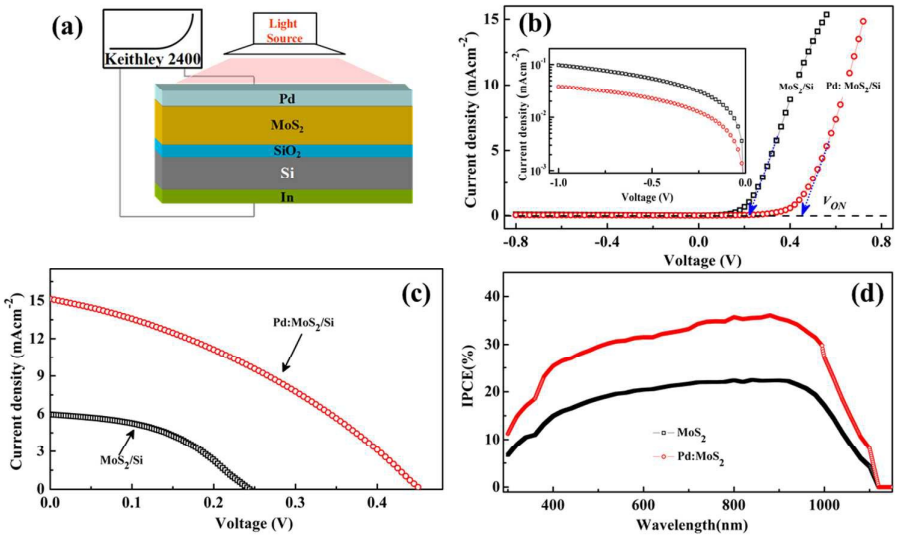

Fig. 3 (a) Schematic illustration of the measurement configuration for photovoltaic measurements. (b) Dark *J-V* curves of the fabricated devices with/without Pd doping in the MoS_2 films. The inset shows the replots of the dark *J-V* curves in the reverse voltage range using semi-logarithmic mode. (c) Photovoltaic characteristics of the solar cell devices with/without Pd doping in the MoS_2 films under AM1.5. (d) Corresponding incident photon-to-electron conversion efficiency curves of the solar cells.

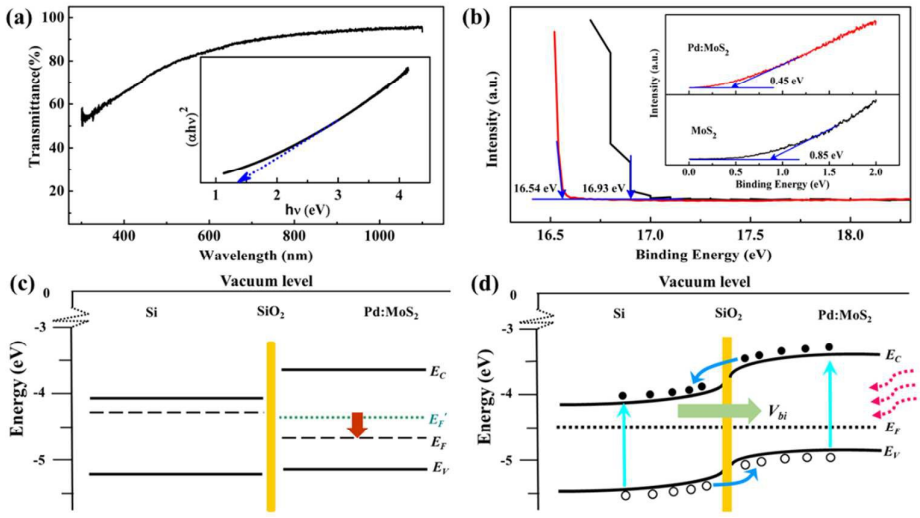

Fig. 4 (a) Transmission spectrum of the Pd:MoS_2 thin film. The inset shows a plot of $(\alpha h\nu)^2$ versus hν. (b) UPS spectra of the undoped and doped MoS_2 film on Si, showing the Fermi level of the films and the distance between the Fermi level and the top edge of the conduction band, respectively. (c) and (d) Energy band diagram before and after contact Pd:MoS_2/Si devices, respectively. The Fermi level (E_F') of the undoped MoS_2 film is also shown in (c) as a comparison with that for the doped film and the red arrow illustrates the change of the Fermi level due to the Pd doping in the film.

RSC Advances

COMMUNICATION

Fig. 4a shows the transmission spectrum of the Pd:MoS_2 thin film. As shown in the figure, the transmittance of the film decreases with decreasing the wavelength in the whole measurement range of 1100-300 nm. Using the data from the spectrum, $(\alpha h\nu)^2$ is plotted as a function of photon energy hν, wherein h, ν and α represent the Planck constant, photon frequency and the absorption coefficient, respectively.[16] The band gap (E_g) of the film can be determined by the intercept of the line on hν axis, E_g=1.37 eV. Fig. 4b shows the UPS spectrum of the MoS_2 films with/without the Pd doping. The work function (W) of the films can be calculated from the difference between the cutoff of the highest binding energy and the photon energy of the exciting radiation. From the figure, W=4.29 eV for the pure MoS_2 film and W=4.68 eV for the Pd:MoS_2 film can be obtained. The distance (ΔE) between the valence band (E_V) and the Fermi level (E_F) of the films can be extracted from the onset energy, as shown in the inset. The ΔE for the films with/without the Pd doping can be determined to be 0.45 and 0.85 eV, respectively. According to above analysis, the *n*-type behavior for the pure MoS_2 film can be proved, however, the Pd:MoS_2 film is *p*-type. This is consistent with the XPS results in Fig. 2c. The *p*-type nature of the Pd:MoS_2 film might be caused by the stronger electronegativity of Pd (2.20) than Mo (2.16). The larger electronegativity of the Pd atoms makes it more difficult for S to receive the electrons from Pd. This can cause large quantities of vacancies in the MoS_2 film and the native electron carriers can be compensated. As a result, the Fermi level of the doped film move towards E_V and *p*-type characteristics are exhibited. The Fermi level of *n*-type Si is 4.21 eV, and its electron affinity and band gap are respectively 4.05 eV and 1.12 eV.[17] Based on above results, the isolated energy-band diagrams of the Pd:MoS_2 film and Si are constructed, as shown in Fig. 4c. In the figure, the Fermi leverl (E_F') of the MoS_2 film was comparatively supplied in the diagram and the red-colored arrow illustrates the shift of E_F caused by the Pd doping. Additionally, the SiO_2 layer as the surface passivation layer is incorporated into the interface in the figure. When the Pd:MoS_2 film is deposited onto the Si substrate, the electrons flow from the substrate into the film at the interface due to the higher E_F of the Si. The flowing process stops when the Fermi levels are equal and the Pd:MoS_2/Si *p-n* junction is fabricated, as shown in Fig. 4d. Consequently, a built-in electrical field (E_{bi}) is formed near the interface and its direction points from the substrate to the film. Thus, asymmetric characteristics and obvious rectifying effect can be observed from the *J-V* curve in Fig. 3b. Under the light illumination, the incident photons generate the electron-hole (e-h) pairs in the Pd:MoS_2 film and Si. The E_{bi} can effectively facilitate the separation of photo-generated e-h pairs, transporting separated electrons from Pd:MoS_2 to Si and holes towards Si by passing the SiO_2 thin layer through tunneling.[18] The processes of photo-excitation and carrier transport in the Pd:MoS_2/Si *p-n* junction are demonstrated in the figure. Therefore, obvious photovoltaic characteristics are exhibited in the Pd:MoS_2/Si *p-n* junction. In a solar cell device, the V_{OC} depends on the V_{bi}.[19] According to semiconductor theory about *p-n* junction,[20] V_{bi} is equal to the difference of the Fermi levels between the joining sides of the junction. As shown in Fig. 4b, the larger work function for the Pd:MoS_2 film demonstrates that the Fermi level of the MoS_2 film can be shifted towards the valence band when the Pd dopants are incorporated into the film, as illustrated in Fig. 4c. This results that the E_{bi} near the Pd:MoS_2/Si interface can be enhanced by the Pd doping. According the work function from the UPS results, E_{bi}=0.47 V for the Pd:MoS_2/Si junction while only 0.08 V for the undoped junction. Thus, the Pd:MoS_2/Si device shows a larger V_{OC} of 0.45 V compared to the device without the Pd doping. Simultaneously, the large V_{bi} at the Pd:MoS_2/Si interface can further promote the separation and facilitate the transportation of the photo-generated carriers, leading to the increase of the J_{SC} from 5.9 mAcm^{-2} to 15.1 mAcm^{-2}. Consequently, the large increase of the PCE of the device can be achieved in the Pd:MoS_2/Si solar cell.

Conclusions

In summary, Pd:MoS_2/Si solar cells were fabricated using magnetic sputtering technique. Due to the incorporation of the Pd atoms, the photovoltaic characteristics of the fabricated solar cell were enhanced significantly. Under AM 1.5 illumination, V_{OC} increased from 0.22 V to 0.45 V and the J_{SC} increased from 5.9 to 15.1 mAcm^{-2}, resulting a 375% enhancement of the PCE to 2.4%. According to the obtained results, the improved device performance could be mainly attributed to the modulation of the Pd doping on the energy-band structures of the MoS_2 films.

Acknowledgements

The authors would like to acknowledge the financial support by the Fundamental Research Funds for the Central Universities (14CX05038A and 15CX08009A) and the National Natural Science Foundation of China (Grant No. 51502348, 51102284 and 51372030).

Notes and references

1 M. Bernardi, M. Palummo and J. C. Grossman, *Nano Lett.*, 2013, **13**, 3664; M. M. Furchi, A. Pospischil, F. Libisch, J. Burgdörfer and T. Mueller, *Nano Lett.*, 2014, **14**, 4785.

2 R. Cheng, D. Li, H. Zhou, C. Wang, A. Yin, S. Jiang, Y. Liu, Y. Chen, Y. Huang and X. Duan, *Nano Lett.*, 2014, **14**, 5590; M. Shanmugam, C. A. Durcan and B. Yu, *Nanoscale*, 2012, **4**, 7399; M. Fontana, T. Deppe, A. K. Boyd, M. Rinzan, A. Y. Liu, M. Paranjape and P. Barbara, *Scientific Rep.*, 2013, **3**, 1634.

3 S. Wi, H. Kim, M. Chen, H. Nam, L.J Guo, E. Meyhofer and X. Liang, *ACS Nano*, 2014, **8**, 5270.
4 L. Wang, J. Jie, Z. Shao, Q. Zhang, X. Zhang, Y. Wang, Z. Sun and S. T. Lee, *Adv. Funct. Mater.*, 2015, **25**, 2910.
5 M. L. Tsai, S. H. Su, J. K. Chang, D. S. Tsai, C. H. Chen, C. I. Wu, L. J. Li, L. J. Chen and J. H. He, *ACS Nano*, 2014, **8**, 8317.
6 Y. Tsuboi, F. Wang, D. Kozawa, K. Funahashi, S. Mouri, Y. Miyauchi, T. Takenobu and K. Matsuda, *Nanoscale* 2015, **7**, 14476.
7 S. Chuang, C. Battaglia, A. Azcatl, S. McDonnell, J. S. Kang, X. Yin, M. Tosun, R. Kapadia, H. Fang, R.M. Wallace and A. Javey, *Nano Lett.*, 2014, **14**, 1337; J. D. Lin, C. Han, F. Wang, R. Wang, D. Xiang, S. Qin, X. Zhang, L. Wang, H. Zhang, A. T. S. Wee and W. Chen, *ACS Nano*, 2014, **8**, 5323; S. Tongay, J. Zhou, C. Ataca, J. Liu, J. S. Kang, T. S. Matthews, L. You, J. Li, J. C. Grossman and J. Wu, *Nano Lett.*, 2013, **13**, 2831 ; K. K. Tiong, P. C. Liao, C. H. Ho and Y. S. Huang, *J. Crystal Growth,* 1999, **205**, 543; J. Suh, T. E. Park, D. Y. Lin, D. Fu, J. Park, H. J. Jung, Y. Chen, C. Ko, C. Jang, Y. Sun, R. Sinclair, J. Chang, S. Tongay and J. Wu, *Nano Lett.*, 2014, **14**, 6976.
8 D. Kiriya, M. Tosun, P. Zhao, J. S. Kang and A. Javey, *J. Am. Chem. Soc.*, 2014, **136**, 7853; H. T. Wang, Z. Y. Lu, D. S. Kong, J. Sun, T. M. Hymel and Y. Cui, *ACS Nano*, 2014, **8**, 4940.
9 M. Ma, Q. Xue, H. Chen, X. Zhou, D. Xia, C. Lv and J. Xie, *Appl. Phys. Lett.*, 2010, **97**, 061902.
10 D. J. Late, P. A. Shaikh, R. Khare, R. V. Kashid, M. Chaudhary, M. A. More and S. B. Ogale, *ACS Appl. Mater. Interfaces*, 2014, **6**, 15881.
11 L. Yuwen, F. Xu, B. Xue, Z. Luo, Q. Zhang, B. Bao, S. Su, L. Weng, W. Huang and L. Wang, *Nanoscale*, 2014, **6**, 5762.
12 J. Ye and C. Liu, *Chem. Commun.*, 2011, **47**, 2167.
13 S. McDonnell, R. Addou, C. Buie, R. M. Wallace and C. L. Hinkle, *ACS Nano*, 2014, **8**, 2880.
14 S. Walia, S. Balendhran, Y. Wang, R. A. Kadir, A. S. Zoolfakar, P. Atkin, J. Z. Ou, S. Sriram, K. Kalantar-zadeh and M. Bhaskaran, *Appl. Phys. Lett.*, 2013, **103**, 232105.
15 L. Z. Hao, Y. J. Liu, W. Gao, Z. D. Han, Q. Z. Xue, H. Z. Zeng, Z. P. Wu, J. Zhu and W. L. Zhang, *J. Appl. Phys.*, 2015, **117**, 114502.
16 X. Chen, K. Ruan, G. Wu and D. Bao, *Appl. Phys. Lett.*, 2008, **93**, 112112.
17 K. Jiao, C. Duan, X. Wu, J. Chen, Y. Wang and Y. Chen, *Phys. Chem. Chem. Phys.*, 2015, **17**, 8182.
18 L. Z. Hao, W. Gao, Y. J. Liu, Z. D. Han, Q. Z. Xue, W. Y. Guo, J. Zhu and Y. R. Li, *Nanoscale*, 2015, **7**, 8304.
19 J. Shewchun, J. Dubow, A. Myszkowski and R. Singh, *J. Appl. Phys.*, 1978, **49**, 855.
20 S. M. Sze and K. K. Ng, *Physics of Semiconductor Devices*, Wiley, New York, 3rd edn, 2007.

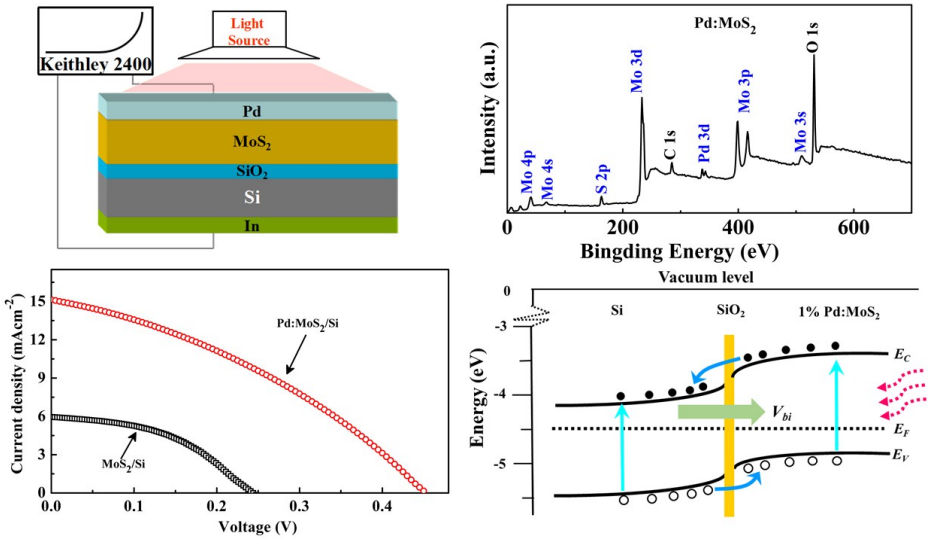

MoS_2/Si hybrid solar cells are fabricated and the device performances are improved via metal Pd chemical doping. Due to the incorporation of the Pd atoms, the photovoltaic characteristics of the fabricated Pd:MoS_2/Si solar cell are enhanced significantly. The open-circuit voltage increases by 2-fold to 0.45 V and the short-circuit current intensity increases from 5.9 to 15.1 $mAcm^{-2}$, resulting a 375% enhancement of the power conversion efficiency to 2.4%. The mechanisms of the improved device performance are clarified by the determination of the energy-band alignment near the Pd:MoS_2/Si interface.